Controlling Band Gap Energies in Cluster-Assembled Ionic Solids through Internal Electric Fields

Nirmalya K. Chaki,[†] Sukhendu Mandal,[†] Arthur C. Reber,[§] Meichun Qian,[§] Hector M. Saavedra,[†] Paul S. Weiss,[†,‡,⊥,*] Shiv N. Khanna,[§,*] and Ayusman Sen[†,*]

[†]Department of Chemistry and [‡]Department of Physics, The Pennsylvania State University, University Park, Pennsylvania 16802, United States, [§]Department of Physics, Virginia Commonwealth University, Richmond, Virginia 23284, United States, and [⊥]California NanoSystems Institute, Department of Chemistry and Biochemistry, and Department of Materials Science and Engineering, University of California, Los Angeles, Los Angeles, California 90095, United States

ABSTRACT Assembling ionic solids where clusters are arranged in different architectures is a promising strategy for developing band gap-engineered nanomaterials. We synthesized a series of cluster-assembled ionic solids composed of $[As_7-Au_2-As_7]^{4-}$ in zero-, one-, and two-dimensional architectures. Higher connectivity is expected to decrease the band gap energy through band broadening. However, optical measurements indicate that the band gap energy increases from 1.69 to 1.98 eV when moving from zero- to two-dimensional assemblies. This increase is a result of the local electric fields generated by the adjacent counterions, which preferentially stabilize the occupied cluster electronic states.

KEYWORDS: cluster-assembled materials · arsenic clusters · band gap tuning

A promising discovery in the field of clusters and nanoscience is the development of nanoscale materials with clusters as building blocks. As the properties of clusters change with size and composition, cluster assemblies offer the attractive proposition of forming materials with novel properties.[1−14] Many cluster solids involve building motifs coupled by linkers and offer unusual properties because they are marked by intra- and intercluster and linker−cluster interactions and length scales, unavailable in atomic solids.[3] Also, the electronic properties of a cluster solid will depend on both the electronic states of individual clusters as well as the longer range interactions found after incorporating the clusters into a material. The electronic structures of cluster solids may be very different from free clusters, for example, the gap between the highest occupied molecular orbital (HOMO) and the lowest unoccupied molecular orbital (LUMO) in a free Li_3As_7 cluster is 2.86 eV, while the band gap of the corresponding solid is only 0.52 eV.[3] Consequently, to understand the origins of properties in these cluster solids, the interactions that control the relationship between the electronic states of the cluster and linkers and the nearby clusters must be characterized. This relationship has led to novel properties, such as the superconducting transition temperature of alkali-doped fullerides,[1] magnetism in assemblies of nonmagnetic elements,[2] and tunable band gap energies in assemblies made from As_7^{3-} motifs.[15] In fact, Zintl phases[16] consisting of polyvalent anions ionically linked *via* strong ionic interactions with cations sometimes exhibit semiconducting or metallic behaviors. Here, we demonstrate a new manifestation of this interplay in ionic cluster assemblies; the cluster's electronic structure can be altered by the ionic linkers, which can lead to unexpected behaviors.

In this work, we study ionic cluster assemblies built out of covalently linked multicenter building blocks of $[As_7-Au_2-As_7]^{4-}$ composed of two As_7 units linked by Au atoms. The covalent linking not only changes the oxidation state of the composite cluster[17−23] to −4 but also allows assemblies of various dimensionalities through choice of alkali counterions that directly link the multiply charged clusters and sequestering agents that capture ions and reduce the dimensionality. This enables a comprehensive study of the effect of varying the architecture on the properties of the assembly, thereby providing insights that may be applied to other ionic nanoscale assemblies. Since clusters have delocalized orbitals with differing orientations, different regions of the electronic spectrum are affected differently by the presence of the electric field generated by the cations. We find that two-dimensional arrangements have higher band gap energies than zero- and one-dimensional assemblies because of the large localized electric field generated by

*Address correspondence to psw@cnsi.ucla.edu, snkhanna@vcu.edu, asen@chem.psu.edu.

Received for review July 14, 2010 and accepted September 23, 2010.

Published online September 30, 2010.
10.1021/nn101640r

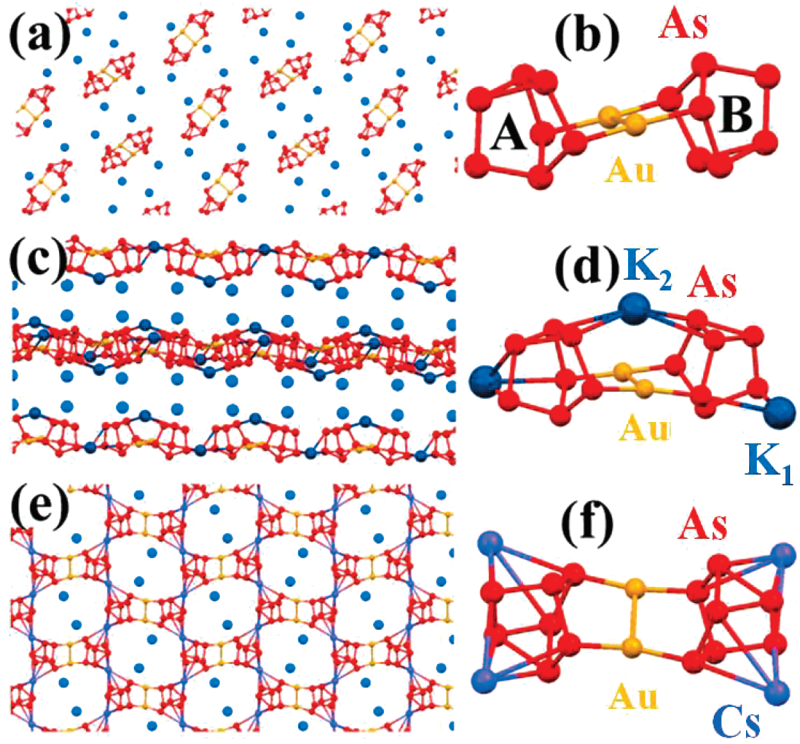

Figure 1. (a) $[Au_2(As_7)_2]^{4-}$ and $(K\text{-Crypt})^+$ in 1 viewed along the *b* axis. (b) $[Au_2(As_7)_2]^{4-}$, two arsenic clusters A and B linked through a gold dimer in 1. (c) One-dimensional arrangement of 2 as viewed along the *b* axis. (d) Two different naked K^+ cations with $[Au_2(As_7)_2]^{4-}$ in 2. (e) Two-dimensional distorted honeycomb-like layers of $[Au_2(As_7)_2]^{4-}$ linked by Cs^+ in 4 as viewed along the *a* axis. (f) Cs^+ cations with $[Au_2(As_7)_2]^{4-}$ in 4. As is red, Cs is purple, K is blue, and Au is gold; the crypt is not shown.

the counterions that preferentially stabilize the states at the top of the valence band.

RESULTS AND DISCUSSION

In this study, we synthesized multiple counterion-directed architectures of $[As_7Au_2As_7]^{4-}$ as (**1**) $Au_2(As_7)_2(K\text{-Crypt})_4$, (**2**) $Au_2(As_7)_2K_2(K\text{-Crypt})_2$, (**3**) $Au_2(As_7)_2Rb_2(Rb\text{-Crypt})_2$, (**4**) $Au_2(As_7)_2Cs_2(K\text{-Crypt})_2$, and (**5**) $Au_2(As_7)_2Cs_2(Rb\text{-Crypt})_2$. "Crypt" is the sequestering agent 4,7,13,16,21,24-hexaoxa-1,10-diazabicyclo[8.8.8]hexacosane. The structures of the resulting solids were characterized through X-ray diffraction, and pertinent experimental details of **1**−**5** are presented in Table S1, Supporting Information. Figure 1 shows the X-ray crystallographic structures of **1**, **2**, and **4** and the interaction of $[As_7Au_2As_7]^{4-}$ with naked alkali metal cations. Compounds **1**−**5** all have the same basic building $[As_7Au_2As_7]^{4-}$, but changing the cation results in zero- (**1**), one- (**2**), and two-dimensional (**3**−**5**) architectures (Figure 1 and Figures S1−3, Supporting Information). The structure of the $[Au_2(As_7)_2]^{4-}$ consists of two As_7, A (left) and B (right), bonded to either side of the Au dimer (Figure 1b). A comparison of the structures of **1**−**5** also reveals the flexible combinatorial nature of As_7 and Au_2 fragments, which can adopt different orientations depending on the specific countercation size (K^+ as compared to Rb^+ and Cs^+). For example, the arrangements of the As_7 units with respect to Au dimers are found to be identical in **1** and **3**−**5** but different in **2** (Figure 1 and Figures S1−3, Supporting Information). In particular, arrangements of the two As_7 units are similar with respect to the Au dimer in **2**, while they are oppositely oriented in **1** and **3**−**5**. The Au−As bond distances of **1**−**5** are found to be in the range of 2.43−2.46 Å, which is in the typical range for Au−As bonds.[24] Also an axial Au−Au bond is observed, rang-

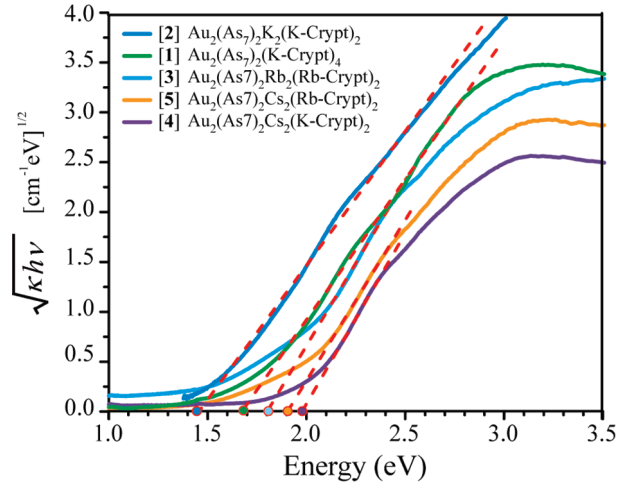

Figure 2. Tauc plots showing the band gap energies determined from the optical absorption spectra (see text) of (1) $Au_2(As_7)_2(K\text{-Crypt})_4$, (2) $Au_2(As_7)_2K_2(K\text{-Crypt})_2$, (3) $Au_2(As_7)_2Rb_2(Rb\text{-Crypt})_2$, (4) $Au_2(As_7)_2Cs_2(K\text{-Crypt})_2$, and (5) $Au_2(As_7)_2Cs_2(Rb\text{-Crypt})_2$.

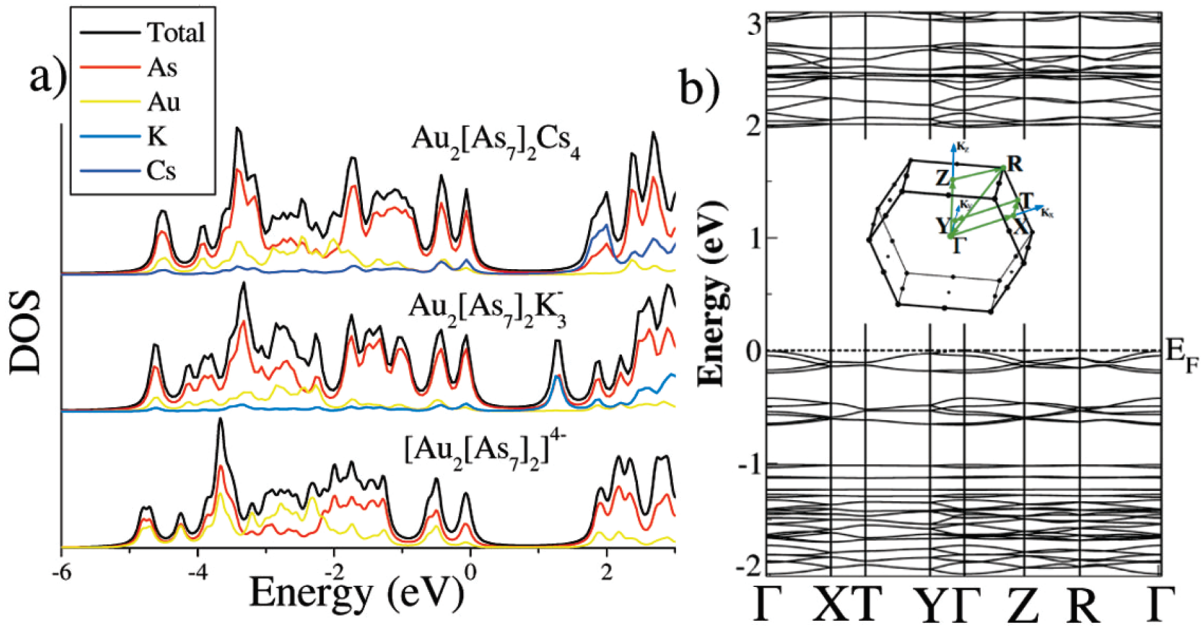

Figure 3. (a) Calculated DOS and projected DOS on each atom for cluster models of 1, 2, and 4, broadened by 0.075 eV Lorentzians. (b) Calculated band structure of 4, where the two-dimensional plane corresponds to $Y-\Gamma$.

ing from 3.08−3.11 Å, and is thus in the range of "aurophilic" contact.[25] The detailed comparison of bond distances of As−As, As−Au, and Au−Au of **1**−**5** are summarized in Tables S2−S6, Supporting Information.

To demonstrate the effect of architecture on properties, we measured the optical band gap energies of **1**−**5** using diffuse reflectance spectroscopy and analysis from the Kubelka−Munk model.[26,27] This two-flux model, which considers only diffuse light, has been widely used to treat the absorption coefficients from surfaces. For a crystalline solid with band gap energy (E_{bg}), the frequency dependence (ν) of the absorption coefficient (κ) can be approximated as:

$$\kappa(\nu) = \frac{B_T(h\nu - E_{bg})^n}{h\nu} \quad (1)$$

where B_T is a constant derived from the square of the averaged dipolar momentum matrix element, and n is equal to 0.5 and 2 for direct and indirect band gap transitions, respectively.[26,27] Using eq 1, the band gap energy of a material can be obtained with a linear fit to a plot of $(\kappa h\nu)^{1/n}$ vs $h\nu$ and extrapolating to zero. Figure 2 shows these Tauc plots for the measured cluster assemblies. The band gap energies were determined using the formula for indirect transitions and are listed in Table 1. Note that the band gap energy of the zero-dimensional assembly (**1**) is 1.69 eV; however, in one-dimensional assemblies (**2**), the energy gap decreased to 1.46 eV but increased to 1.87, 1.97, and 1.98 eV for two-dimensional assemblies (**3**−**5**, respectively).

TABLE 1. Experimentally Measured and Theoretically Calculated Band Gap Energies of $[Au_2(As_7)_2]^{4-}$-Based Cluster Assemblies

	compound	expt. band gap (eV)	theor. band gap (eV)
1	$Au_2(As_7)_2(K\text{-Crypt})_4$	1.69 ± 0.02	1.68
2	$Au_2(As_7)_2K_2(K\text{-Crypt})_2$	1.46 ± 0.02	1.43
3	$Au_2(As_7)_2Rb_2(Rb\text{-Crypt})_2$	1.87 ± 0.05	2.09
4	$Au_2(As_7)_2Cs_2(K\text{-Crypt})_2$	1.97 ± 0.01	2.06
5	$Au_2(As_7)_2Cs_2(Rb\text{-Crypt})_2$	1.98 ± 0.05	2.00

First principles electronic structure studies were carried out to examine the nature of the electronic states. The geometry and unit cell determined from the X-ray crystal structure were used, and the band gap energies and electronic bands in the periodic solid were calculated with the Vienna *ab initio* simulation package (VASP)[28] using a gradient corrected functional.[29] The theoretical band gap energies are summarized in Table 1 and are compared with their experimental values. The calculated band gap energies are in good agreement with the corresponding experimentally measured band gap energies, a consequence of the weak interactions between clusters, which results in localized cluster states that are well-described within density functional theory.[30] Further, Figure 3a shows the comparison of the calculated density of states (DOS) and projected DOS on each atom for the $[Au_2(As_7)_2]^{4-}$, $K_3[Au_2(As_7)_2]^-$, and $Cs_4[Au_2(As_7)_2]$ cluster models[31] corresponding to **1**, **2**, and **4**, while Figure 3b shows the representative band structure of **4**. Next, we analyze the effect of architecture on the electronic properties of **1**−**5,** starting from zero- (**1**), one- (**2**), and finally two- (**3**−**4**) dimensional cluster assemblies.

The $[Au_2(As_7)_2]^{4-}$ units are arranged in a zero-dimensional fashion in **1,** where none of these clusters interact with another. The experimental band gap energy of this material is found to be 1.69 eV and is in good agreement with the theoretically calculated value

of 1.68 eV. In this solid, the top of the valence band and bottom of the conduction band consist of As and Au states, respectively, as the K-Crypt states are pushed up and buried deep into the conduction band (Figure 3a). The zero-dimensional solid **1** has the intrinsic band gap energy of an isolated $[Au_2(As_7)_2]^{4-}$ motif and can be used to guide understanding of the band gap energies in assemblies with higher connectivity. In **2**, $[Au_2(As_7)_2]^{4-}$ forms a linear one-dimensional chain by interacting with two naked K^+ ions. The experimental band gap energy is found to be 1.46 eV and is in good agreement with the calculated value of 1.43 eV. The band gap energy of **2** is less than **1**, which can be explained by the nature of the counterion in **2**. The HOMO of the neutral alkali atom determines the bottom of the conduction band of the cluster solid,[3] and the energy of the HOMO of the neutral K atom is significantly lower than that of the K-Crypt. This results in a smaller band gap energy in **2**, which is seen in Figure 3a in which the DOS projected from the K atom inserts into the gap of **2**.

The structures of **3**−**5** are two-dimensional layers formed by interactions of naked Rb^+ (**3**) and Cs^+ (**4** and **5**) with $[Au_2(As_7)_2]^{4-}$, while cryptated alkali cations separate these layers. The band gap energies of **3**−**5** are found to be 1.87, 1.97, and 1.98 eV, respectively, and are in good agreement with the theoretically calculated values of 2.09, 2.06, and 2.00 eV for **3**−**5**, respectively. Comparable values of band gap energies are expected for **3**−**5** due to similar architecture. The striking result is that the band gap energies for all of the two-dimensional assemblies (**3**−**5**) are larger than the band gap energy of the zero-dimensional assembly (**1**), whose band gap energy is expected to be the upper limit. How then does varying the architecture of the assembly increase the band gap energy to a larger value than that of an isolated cluster motif?

We first consider the effect of architectural change on different interactions that the clusters may experience. In conventional solids, moving from a lower to a higher dimensional structure results in broadening of the valence and conduction bands, resulting in a smaller gap. Here, the band widths of the cesium-linked (**4**) ionic cluster solids is 0.14 eV (as seen in Figure 3), so broadening does not significantly affect the band gap energy. The small band widths are due to weak direct overlap of electronic states in neighboring clusters as they are separated by cations. Changing the dimensionality of the ionic clusters assemblies, however, will change the long-range structure of the lattice and vary the depth of the electrostatic potential. The Madelung constant of the solid may also affect the total stability of the assembly, but it would not affect the band gap energy. Long-range electronic interactions act like a Faraday cage, where changing the depth of the potential shifts all electronic states equally and thus leaves the band gap energy unaffected. A significant local gradient in the electrostatic potential near the cluster, which modulates the electronic structure of the individual motifs, could be responsible for the unexpected band gap energy increase for the two-dimensional cluster solids.

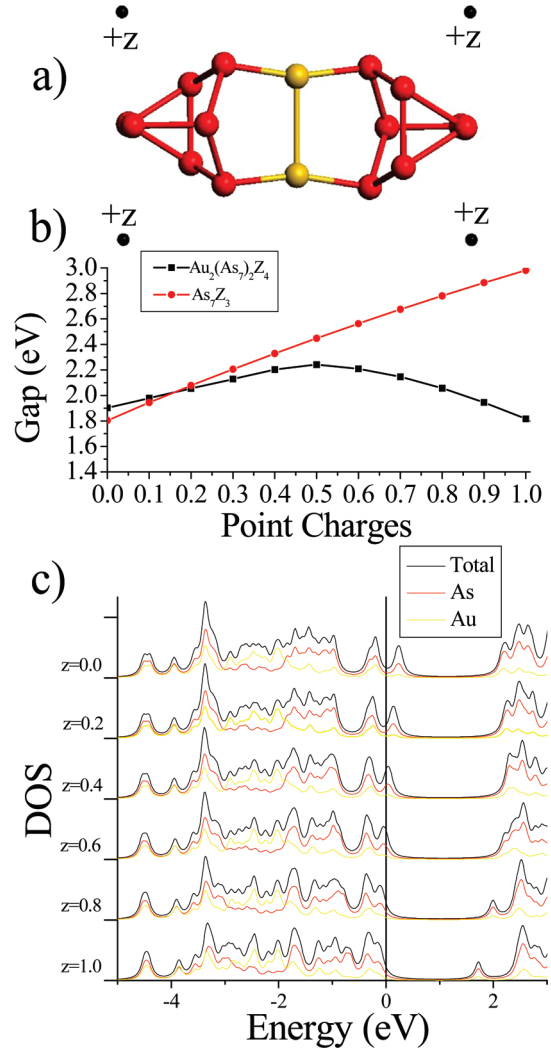

Figure 4. (a) Positions of point charges in the cluster model, (b) variation of the band gap energies, and (c) projected DOS as a function of the point charges. The shifts are relative to the 5s core state of Au.

We hypothesize that the counterions that are adjacent to the clusters generate an electric field that can significantly alter the local gradient of the electrostatic potential near the cluster motif. To demonstrate this, we calculated the electronic structure for an isolated $[Au_2(As_7)_2]^{4-}$ cluster (Figure 4a) with four point charges, *z*, placed at the same positions as Cs in the solid. The strength of the positive charges was varied from 0.0 to +1.0e, and we monitored the variation of the HOMO−LUMO gap as well as the location of the HOMO and LUMO. The gaps were found to increase smoothly by 0.34 eV when varying the point charge from 0 to +0.5e and then to decrease with higher fields. The DOS was also examined as a function of electric field; the results are shown in Figure 4c. We found that the in-

crease in the HOMO−LUMO gap is caused by the stabilization of the HOMO with the increasing field, while the LUMO states show little change until $z = +0.6$ e. Further increased electric fields reduce the gap as the As−Au mixed states are strongly stabilized to become the LUMO at high field. Similar electric field-dependent behavior is also observed for the case of As_7^{3-} clusters, however the gap increases monotonically from $z = 0.0$ to +1.0 e (Figure 4b). These results show that the band gap energies of the two-dimensional ionic solids (**3**−**5**) increase due to the generation of internal electric fields by the adjacent counterions.

We also examined the local electrostatic environment of other architectures to show that the internal electric fields are responsible for the increases of the band gap energy in materials **3**−**5**. Figure 5 shows the electrostatic potential of $[(Au_2)(As_7)_2]^{4-}$ and $Cs_4[(Au_2)(As_7)_2]$ as the models for **1** and **4**, respectively, on a plane cut parallel to the Au−As bonds with the associated HOMO plotted as an isosurface. An electric field corresponds to the gradient of the electrostatic potential, so a red to blue sequence indicates a stronger electric field. In $[(Au_2)(As_7)_2]^{4-}$, the electrostatic potential falls off gradually from the isolated cluster because no adjacent counterions are present to generate internal electric fields. In sharp contrast, for the case of $Cs_4[(Au_2)(As_7)_2]$, there is a large electric field generated by the Cs counterions, precisely along the path of the HOMO orbital. Since, the HOMOs generally protrude from the clusters,[10] it is expected that an electric field will generally increase the band gap energy. The band gap energy variation also depends on the precise location of the electric field generated by the counterion and by the charge density of the states near the Fermi energy, so it may not always result in an increase of the band gap energy. Nevertheless, the variation of the electrostatic potentials shows that the band gap energy depends on the local electronic structure and the precise location of the counterions that generate the internal electric field, much like in cluster crystal-field theory.[32,33]

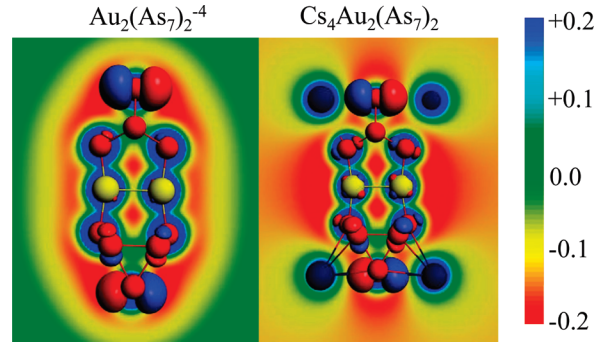

Figure 5. Calculated electrostatic potential of $(As_7)_2Au_2^{4-}$ and $Cs_4(As_7)_2Au_2$ (1 and 4). Potentials are shifted by 0.37 because of different total charges.

CONCLUSIONS

Our results reveal the role of internal electric fields that modulate the band gap energies of ionic cluster-assembled solids. The internal electric fields are generated by closely spaced counterions, whose positions are determined by the architecture of the solid. The variation of band gap energy depends on the precise relationship between the counterions and their ability to stabilize the electronic structure of the clusters and also the absolute value of the alkali metal's HOMO energy state that forms the bottom of the conduction band of the cluster solid. These findings open up a novel protocol for developing band gap-tunable optoelectronic materials by modifying cluster motifs, counterions, and their architectures.

MATERIALS AND METHODS

Synthesis of Cluster Assemblies (Compounds 1−5). All manipulations were performed in an argon-filled glovebox. The precursors, As_7A_3 (A = K, Rb, and Cs), were directly synthesized in ethylenediamine, mixed with the appropriate amount of $AuP(C_6H_5)_3Cl$, and crystallized in presence of crypt to prepare cluster assemblies (**1**−**5**). The suspensions were filtered and layered with toluene or tetrahydrofuran, and after 4−10 days crystals were recovered. Further details about the synthesis of the individual compounds are given in the Supporting Information.

Crystal Structure and Band Gap Determination. For each compound, a crystal was selected and glued to a loop. The X-ray diffraction data were collected using an APEX diffractometer with a CCD area detector at 120 K, and the data were reduced using a procedure outlined in a previous publication.[3] The band gap was determined through diffuse reflectance spectra and analyzed the Kubelka−Munk model for indirect transitions.[26,27] Further details are available in ref 3.

Theoretical Methods. The theoretical studies included two separate investigations using first principles density functional framework. First, studies on the cluster solids were carried out using the Vienna *ab initio* stimulation package (VASP)[28] that uses supercells to simulate the actual material. Here, projector augmented wave (PAW) pseudopotentials[34] were used to describe the electron−ion interaction, while a generalized gradient approximation (GGA)[29] was used for incorporating the exchange interactions and correlations. Brillouin zone integrations were carried out on a Monkhorst−Pack[35] grid *k*-points, using the tetrahedral method. The kinetic energy cutoff of 350 eV is taken for the plane wave basis. The atomic positions were optimized until the forces were less than 10 meV/Å.

To further probe the nature of electronic states in individual building motifs, studies on isolated clusters were carried out using the Amsterdam density functional (ADF) code.[31] These studies used GGA-PBE exchange correlation, with a TZVP basis set, and the zeroth order regular approximation[36] (ZORA) for relativistic effects was used.

Acknowledgment. We thank the U.S. Army Research Office (MURI grant no. W911NF-06-1-0280) and the Kavli Foundation for financial support.

Supporting Information Available: Details on the synthetic methods, procedures for X-ray crystallography and band gap measurements, and crystal data. This material is available free of charge *via* the Internet at http://pubs.acs.org.

REFERENCES AND NOTES

1. Hebard, A. F.; Rosseinsky, M. J.; Haddon, R. C.; Murphy, D. W.; Glarum, S. H.; Palstra, T. T. M.; Ramirez, A. P.; Kortan, A. R. Superconductivity at 18 K in Potassium-Doped C_{60}. *Nature* **1991**, *350*, 600–601.
2. Ugrinov, A.; Sen, A.; Reber, A. C.; Qian, M.; Khanna, S. N. $[Te_2As_2]^{2-}$: A Planar Motif with "Conflicting" Aromaticity. *J. Am. Chem. Soc.* **2008**, *130*, 782–783.
3. Qian, M.; Reber, A. C.; Ugrinov, A.; Chaki, K.; Mandal, S.; Saavedra, H. C.; Khanna, S. N.; Sen, A.; Weiss, P. S. Cluster-Assembled Materials: Towards Nanomaterials with Precise Control Over Properties. *ACS Nano* **2010**, *4*, 235–240.
4. Jadzinsky, P. D.; Calero, G.; Ackerson, C. J.; Bushnell, D. A.; Kornberg, R. D. Structure of a Thiol Monolayer-Protected Gold Nanoparticle at 1.1 Å Resolution. *Science* **2007**, *318*, 430–433.
5. Walter, M.; Akola, J.; Lopez-Acevedo, O; Jadzinsky, P. D.; Calero, G.; Ackerson, C. J.; Whetten, R. L.; Gonbeck, H.; Hakkinen, H. A Unified View of Ligand-Protected Gold Clusters as Superatom Complexes. *Proc. Nat. Acad. Sci. U.S.A.* **2008**, *105*, 9157–9162.
6. Korlann, S. D.; Riley, A. E.; Mun, B. S.; Tolbert, S. H. Chemical Tuning of the Electronic Properties of Nanostructured Semiconductor Films Formed through Surfactant Templating of Zintl Cluster. *J. Phys. Chem. C.* **2009**, *113*, 7697–7705.
7. Sun, D.; Riley, A. E.; Cadby, A. J.; Richman, E. K.; Korlann, S. D.; Tolbert, S. H. Hexagonal Nanoporous Germanium through Surfactant-Driven Self-Assembly of Zintl Clusters. *Nature* **2006**, *441*, 1126–1130.
8. Trikalitis, P. N.; Bakas, T.; Kanatzidis, M. G. Periodic Hexagonal Mesostructured Chalcogenides Based on Platinum and $[SnSe_4]^{4-}$ and $[SnTe_4]^{4-}$ Precursors. Solvent Dependence of Nanopore and Wall Organization. *J. Am. Chem. Soc.* **2005**, *127*, 3910–3920.
9. Banerjee, S.; Szarko, J. M.; Yuhas, B. D.; Malliakas, C. D.; Chen, L. X.; Kanatzidis, M. G. Room Temperature Light Emission from the Low-Dimensional Semiconductors $AZrPS_6$ (A = K, Rb, Cs). *J. Am. Chem. Soc.* **2010**, *132*, 5348–5350.
10. Roach, P. J.; Woodward, W. H.; Castleman, A. W., Jr; Reber, A. C.; Khanna, S. N. Complementary Active Sites are Responsible for the Size-Selective Reactivity of Aluminum Cluster Anions with Water. *Science* **2009**, *323*, 492–495.
11. Castleman, A. W., Jr.; Khanna, S. N.; Sen, A.; Reber, A. C.; Qian, M.; Davis, K. M.; Peppernick, S. J.; Ugrinov, A.; Merritt, M. D. From Designer Clusters to Synthetic Crystalline Nanoassemblies. *Nano Lett.* **2007**, *7*, 2734–2741.
12. Claridge, S. A.; Castleman, A. W., Jr.; Khanna, S. N.; Murray, C. B.; Sen, A.; Weiss, P. S. Cluster-Assembled Materials. *ACS Nano* **2009**, *3*, 244–255.
13. Esenturk, E. N.; Fettinger, J.; Eichhorn, B. W. The Pb_{12}^{2-} and Pb_{10}^{2-} Zintl Ions and the $M@Pb_{12}^{2-}$ and $M@Pb_{10}^{2-}$ Cluster Series Where M = Ni, Pd, Pt. *J. Am. Chem. Soc.* **2006**, *128*, 9178–9186.
14. Hull, M. W.; Sevov, S. C. Functionalization of Nine-Atom Deltahedral Zintl Ions with Organic Substituents: Detailed Studies of the Reactions. *J. Am. Chem. Soc.* **2009**, *131*, 9026–9037.
15. Emmerling, F.; Röhr, C. Alkaline Metal Arsenides A_3As_7 and AAs (A=K, Rb, Cs). Preparation, Crystal Structure, Vibrational Spectroscopy. *Z. Naturforsch., B: J. Chem. Sci.* **2002**, *57*, 963–975.
16. Zintl, E. Intermetallische Verbindungen. *Angew. Chem.* **1939**, *52*, 1–6.
17. Goicoechea, J. M.; Sevov, S. C. $[(Ni\text{-}Ni\text{-}Ni)@(Ge_9)_2]^{4-}$: A Linear Triatomic Nickel Filament Enclosed in a Dimer of Nine-Atom Germanium Clusters. *Angew. Chem., Int. Ed.* **2005**, *44*, 4026–4028.
18. Nienhaus, A.; Hauptmann, R.; Fässler, T. F. $[HgGe_9]_\infty^{2-}$ - A Polymer with Zintl Ions as Building Blocks Covalently Linked by Heteroatoms. *Angew. Chem., Int. Ed.* **2002**, *41*, 3213–3215.
19. Wang, J.-Q.; Stegmaier, S.; Fässler, T. F. $[Co@Ge_{10}]^{3-}$: An Intermetalloid Cluster with Archimedean Pentagonal Prismatic Structure. *Angew. Chem.* **2009**, *121*, 2032–2036.
20. Sun, Z.-M.; Xiao, H.; Li, J.; Wang, L.-S. $Pd_2@Sn_{18}^{4-}$: Fusion of Two Endohedral Stannaspherenes. J. *Am. Chem. Soc.* **2007**, *129*, 9560–9561.
21. Kocak, F. S.; Zavalij, P.; Lam, Y.-F.; Eichhorn, B. W. Solution Dynamics and Gas-Phase Chemistry of $Pd_2@Sn_{18}^{4-}$. *Inorg. Chem.* **2008**, *47*, 3515–3520.
22. Moses, M. J.; Fettinger, J. C.; Eichhorn, B. W. Charged Molecular Alloys: Synthesis and Characterization of the Binary Anions $Pd_7As_{16}^{4-}$ and $Pd_2As_{14}^{4-}$. *J. Am. Chem. Soc.* **2002**, *124*, 5944–5945.
23. Sevillano, P.; Fuhr, O.; Kattannek, M.; Nava, M. P.; Hampe, O.; Lebedkin, S.; Ahlrichs, R.; Fenske, D.; Kappes, M. M. The Phosphine-Stabilized Gold-Arsenic Clusters $[Au_{19}(AsnPr)_8(dppe)_6]Cl_3$, $[Au_{10}(AsnPr)(dppe)_4]Cl_2$, $[Au_{17}(AsnPr)_6(As_2nPr_2)(dppm)_{64}]Cl_3$, and $[Au_{10}(AsPh)_4(dppe)_4]Cl_2$: Synthesis, Characterization, and DFT Calculations. *Angew. Chem. Int. Ed.* **2006**, *45*, 3702–3708.
24. Pyykkö, P. Strong Closed-Shell Interactions in Inorganic Chemistry. *Chem. Rev.* **1997**, *97*, 597–636.
25. Gimeno, M. C.; Laguna, A. Three- and Four-Coordinate Gold(I) Complexes. *Chem. Rev.* **1997**, *97*, 511–522.
26. Kubelka, P. New Contributions to the Optics of Intensely Light Scattering Materials. I. *J. Opt. Soc. Am.* **1948**, *38*, 448–457.
27. Murphy, A. B. Modified Kubelka-Munk Model for Calculation of the Reflectance of Coatings with Optically-Rough Surfaces. *J. Phys. D: Appl. Phys.* **2006**, *39*, 3571–3581.
28. Kresse, G.; Furthmuller, J. Efficient Iterative Schemes for *ab Initio* Total-Energy Calculations Using a Plane-Wave Basis Set. *Phys. Rev. B: Condens. Matter Mater. Phys.* **1996**, *54*, 11169–11186.
29. Perdew, J. P.; Burke, K.; Enzerhof, M. Generalized Gradient Approximation Made Simple. *Phys. Rev. Lett.* **1996**, *77*, 3865–3868.
30. Cohen, A. J.; Mori-Sánchez, P.; Yang, W. Insights into Current Limitations of Density Functional Theory. *Science* **2008**, *321*, 792–794.
31. te Velde, G.; Bickelhaupt, F. M.; van Gisbergen, S. J. A.; Fonseca Guerra, C.; Baerends, E. J.; Snijders, J. G.; Ziegler, T. Chemistry with ADF. *J. Comput. Chem.* **2001**, *22*, 931–967.
32. Hoffman, R.; Gouterman, M. Theory of Polyhedral Molecules. II. A Crystal Field Model. *J. Chem. Phys.* **1962**, *36*, 2189–2195.
33. Roach, P. J.; Woodward, W. H.; Reber, A. C.; Khanna, S. N.; Castleman, A. W., Jr. Crystal Field Effects on the Reactivity of Aluminum-Copper Cluster Anions. *Phys. Rev. B: Condens. Matter Mater. Phys.* **2010**, *81*, 195404.
34. Kresse, G.; J. Joubert, J. From Ultrasoft Pseudopotentials to the Projector Augmented-Wave Method. *Phys. Rev. B: Condens. Matter Mater. Phys.* **1999**, *59*, 1758–1775.
35. Monkhorst, H. J.; Pack, J. D. Special Points for Brillouin-Zone Integrations. *Phys. Rev. B: Solid State* **1976**, *13*, 5188–5192.
36. van Lenthe, E.; Baerends, E. J.; Snijders, J. G. Relativistic Regular Two-Component Hamiltonians. *J. Chem. Phys.* **1993**, *99*, 4597–4610.